Supporting Information

Mechanochemical association reaction of interfacial molecules driven by shear

Arash Khajeh[1], Xin He[2], Jejoon Yeon[1], Seong H. Kim[2], Ashlie Martini[1]

[1] Department of Mechanical Engineering, University of California Merced, 5200 N. Lake Road, Merced, CA 95343, USA

[2] Department of Chemical Engineering and Materials Research Institute, Pennsylvania State University, University Park, Pennsylvania 16802, United States

Activation of the silica substrate surface by rubbing in poorly lubricated condition in experiment

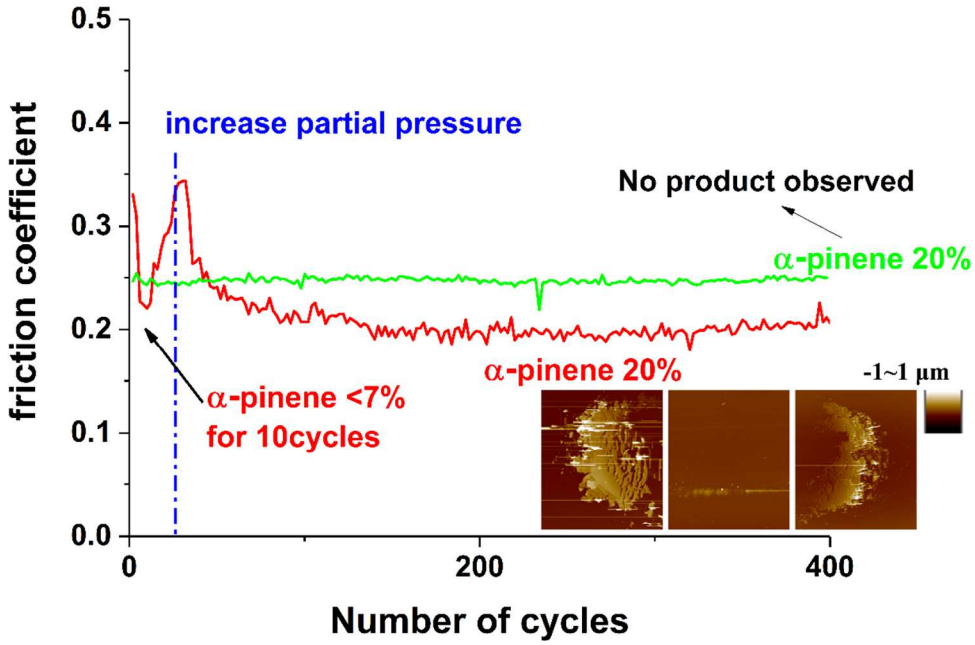

Figure S1. Activation of the hydroxylated surface by friction at a vapor pressure of α-pinene insufficient for monolayer lubrication; when α-pinene vapor pressure was subsequently increased to p/p_{sat} = 40% (sufficient enough for monolayer coverage), shear-induced mechanochemical polymerization occurred more readily compared to the fully hydroxylated original surface.

Water contact angle on fully hydroxylated and thermally dehydroxylated silica surfaces

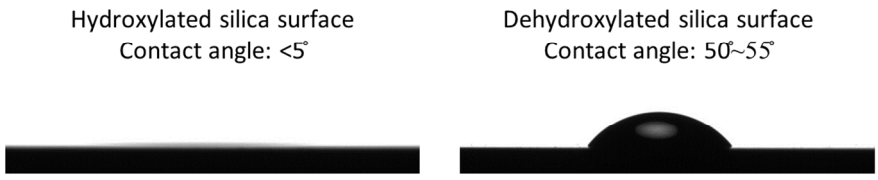

Figure S2. Evidence of dehydroxylation of the UV/O_3-cleaned hydroxylated silica surface upon thermal annealing at 450 ^{o}C for 12 hours. After thermal dehydroxylation, the water contact angle increased from <5^{o} to 50~55^{o}.

Creation of amorphous SiO_2 model structure

The amorphous silica slabs were derived from the cristobalite SiO_2 structure. This crystalline material is a high-temperature form of silica glass that is metastable below 1740 K.[1] The standard method of heating and cooling was used to create the amorphous structure of the two slabs in the sliding model.[2] Figure S3 illustrates the initial and final structures along with the temperature and potential energy during the heating and cooling cycles. The NVT (constant number of atoms, volume and temperature) ensemble was used during heating from room temperature to 4000 K and then cooling down again to 300 K. To minimize strain in the resultant amorphous structure, the heating and cooling rate was fixed at 0.02 K/fs which was the lowest rate possible within the timescale constraints of the simulation.

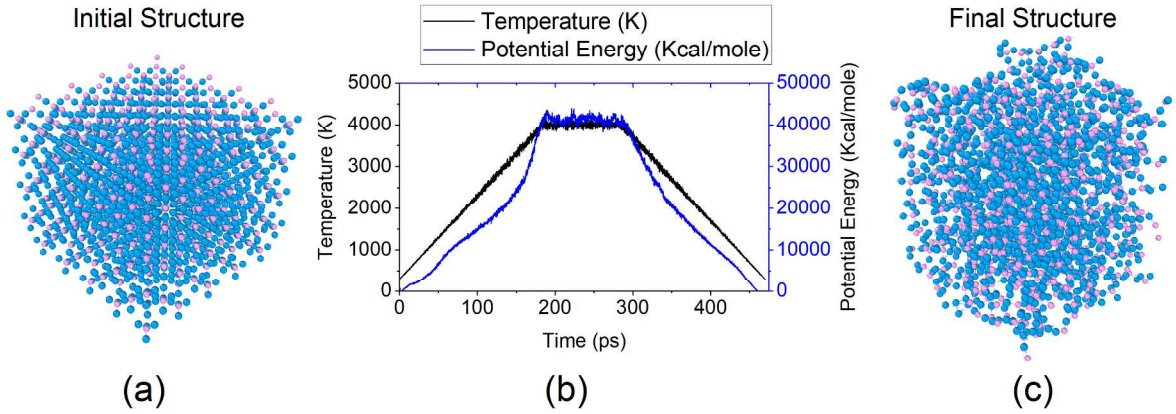

Figure S3. (a) Cristobalite SiO_2, (b) changes in temperature and potential energy during the heating and cooling cycle used to create the amorphous structure, and (c) final structure of the amorphous silica.

The physical data extracted from characterization of the amorphous silica model were compared with those reported in previous studies, as shown in Table S1. All properties calculated for the amorphous structure agreed with the previously reported data within 6% error.

Table S1. Properties of the amorphous silica glass created in this work compared to the results reported in previous MD simulations and experiments.

	This study (from MD simulation)	**Previous MD simulations [3]**	**Experimental values [4-5]**
Bulk density (g/cm^3)	2.1	2.1	2.2
Si-O RDF first peak (Å)	1.58	1.56	1.62
Si-O-Si (degree)	152.0	151.0	144.0
O-Si-O (degree)	110.5	110.0	109.5

Hydroxylation of the model SiO_2 surface

With the aim of creating two systems with different surface reactivities, hydroxylation of the amorphous surface was carried out for one model. Figure S4a shows the model system in which 300 water molecules were added at the top of the amorphous silica (Figure S4a; box size = $3.19 \times 3.19 \times 3.00$ nm^3). Then, the temperature was increased from 300 K to 500 K and NVT simulations were performed for 800 ps. Figure S4b shows the change in the density of silanol groups formed at the surface. The density of silanol groups increased and reached a saturation value at ~300 ps, after which there was negligible change. Lastly, the excess un-reacted water molecules were removed from the system. Figure S5 shows the density of surface functional groups for the non-hydroxylated and hydroxylated models.

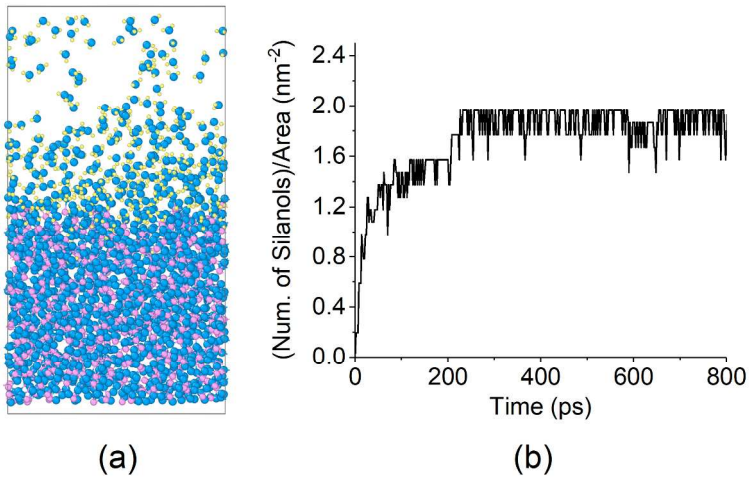

Figure S4. (a) Model system for simulation of hydroxylation. (b) Density of silanol groups on the silica surface during the hydroxylation process.

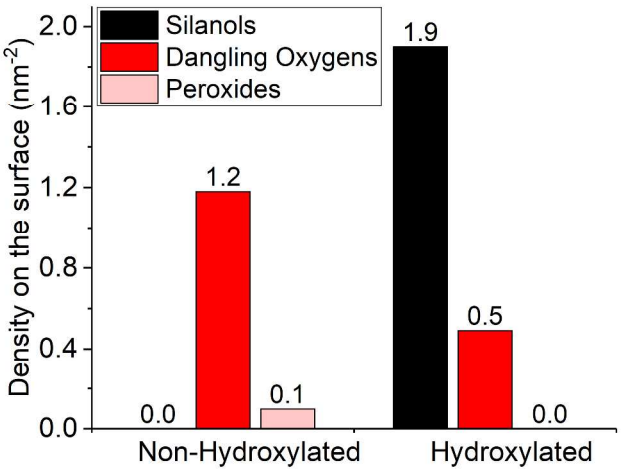

Figure S5. Density of different functional groups on the non-hydroxylated and hydroxylated model silica surfaces.

Pressure dependence of the oligomerization and critical activation volume calculation

Based on the models proposed for the mechanically assisted thermal activation phenomena,[6-10] the rate of reaction (or yield at a constant reaction time) can be expressed as an Arrhenius-type function:

$$r_y = A \exp\left(-\frac{E_a - \sigma \Delta V^*}{k_b T}\right) \quad (1)$$

where r_y is the reaction rate or normalized yield, A is a preexponential factor, E_a is the activation energy barrier for thermal reaction, σ is the applied shear stress, ΔV^* is the critical activation volume, k_b is the Boltzmann constant, and T is the substrate temperature. The shear stress term can be expressed with the applied contact pressure (P) and friction coefficient (α):

$$\sigma = \sigma_0 + \alpha P \quad (2)$$

Here, σ_0 and α are constants. Inserting equation (2) in equation (1) gives:

$$\ln(r_y) = \left(\ln A + \frac{\sigma_0 \Delta V^*}{k_b T} - \frac{E_a}{k_b T}\right) + \frac{\Delta V^* . \alpha}{k_b T} P \quad (3)$$

When the flash temperature increase due to friction is negligible, the terms in the parentheses on the right side of equation (3) would remain constant.[11] Therefore, on a semi-log plot of the reaction yield against the applied pressure, the slope can be used to estimate ΔV^*. In Figure 2c of the main text plotting the normalized yield of mechanochemically produced polymers versus the applied contact pressure, the slope of the linear fit corresponds to $\Delta V^* \approx 8.3$ Å^3.

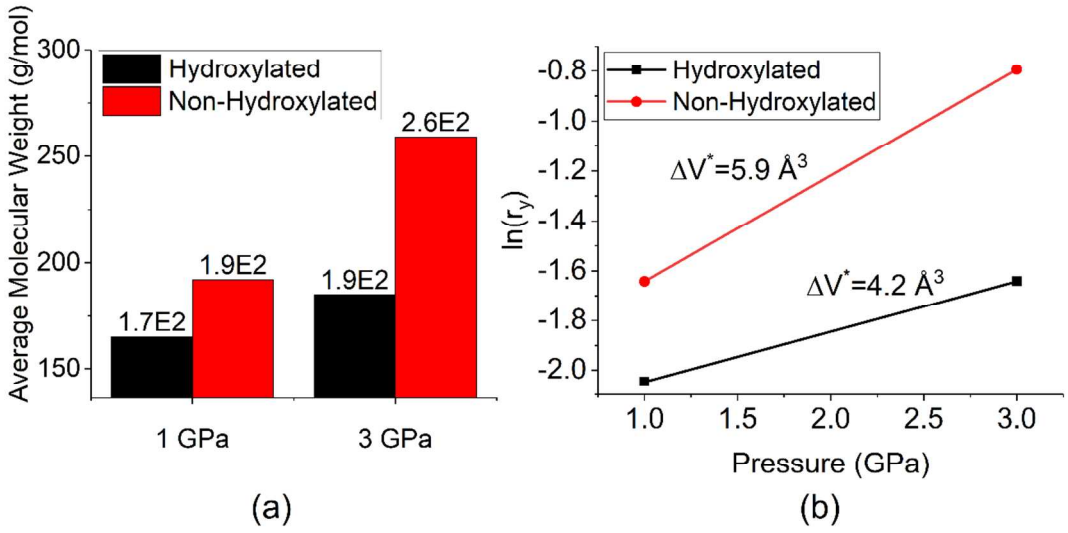

Figure S6. (a) Average molecular weight of reaction products containing more than 10 carbon atoms in MD simulations for the hydroxylated and non-hydroxylated surfaces at contact pressures of 1 GPa and 3 GPa. (b) Calculation of the critical activation volume based on the number of α-pinene molecules associated in simulations at 1GPa and 3GPa conditions.

Figure S6a displays the MD simulation results obtained for two contact pressures: 1 GPa and 3 GPa. Although the statistics in MD simulations are poor due to the limited data set, it is still possible to approximate ΔV^* in simulations using these two data points. Processing the simulation results with equation (3) and the friction coefficient found in the experiment (shown in Figure 2a in the main text) gave the ΔV^* value of ~6 $Å^3$ for the non-hydroxylated surface, which is reasonable when compared with the experimentally determine value (~8.3 $Å^3$). For the hydroxylated surface, it was difficult to get the experimental value because the amount of the reaction products was too small to be measured accurately.

Surface dependence of chemisorption before sliding

In MD simulations, the reaction yield appeared to correlate with the amount of chemisorbed α-pinene species. Figure S7 shows the surface density of α-pinene species before the onset of interfacial shear.

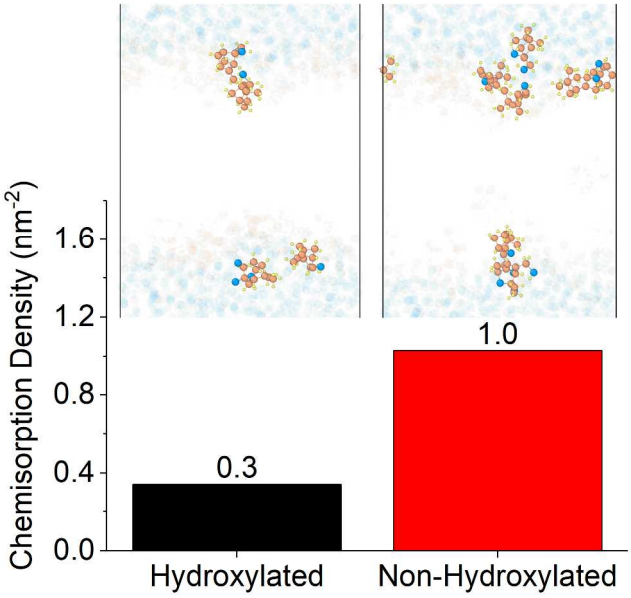

Figure S7. Density of chemisorbed α-pinene molecules on the hydroxylated and non-hydroxylated surfaces at the end of the energy equilibrium step in MD simulations

Association of two molecules via C-O-C bond formation

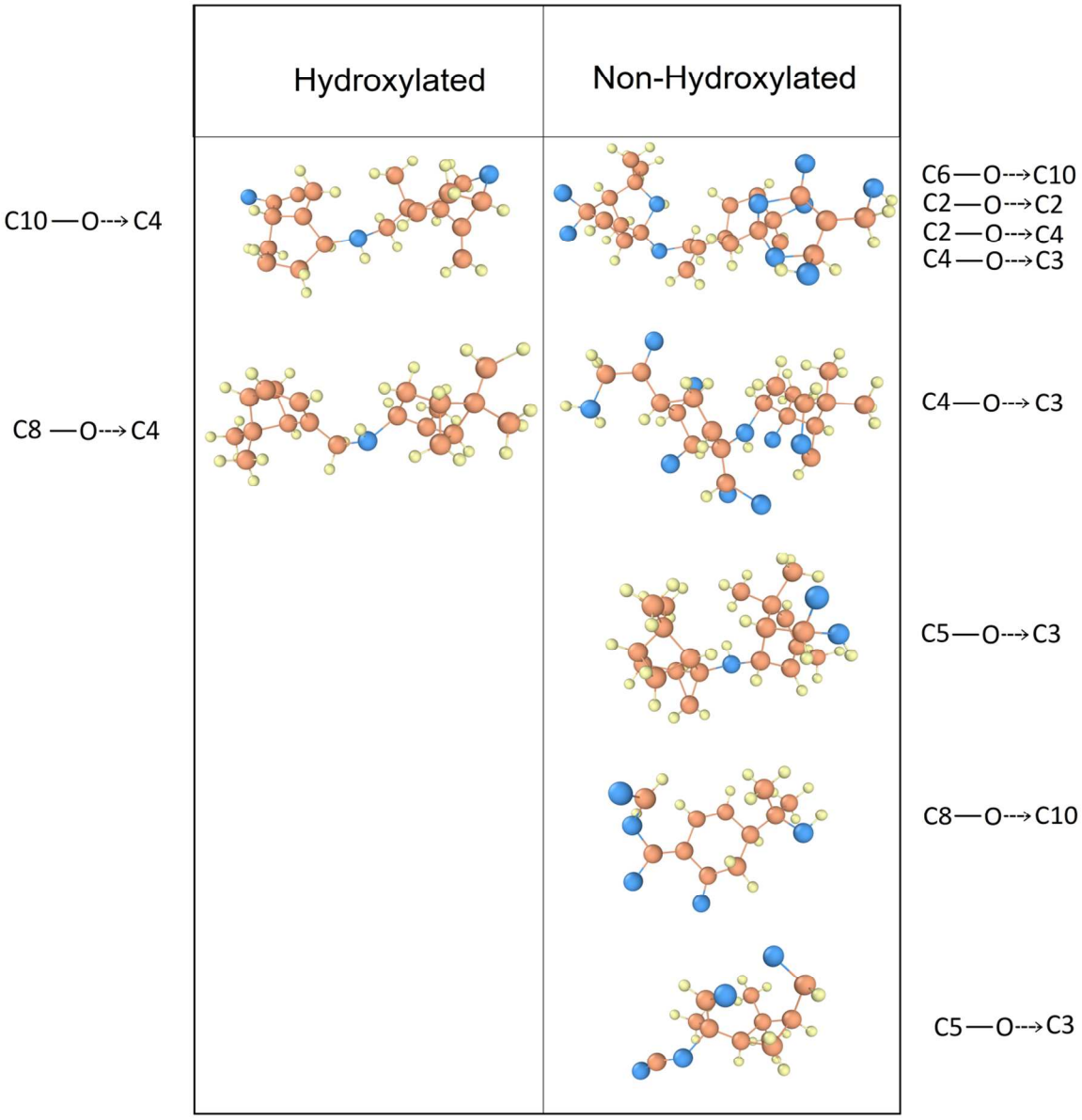

Figure S8. Snapshots of the hydrocarbon species formed in MD simulations with the hydroxylated and non-hydroxylated silica surfaces after 2 ns sliding. The atom numbers at the connection between molecules are provided adjacent to each snapshot. It is important to note that all association products are connected through the C-O-C ether bond; no products were found to be connected via direct C-C covalent bonding.

Comparison of total energy changes for selected reaction pathways

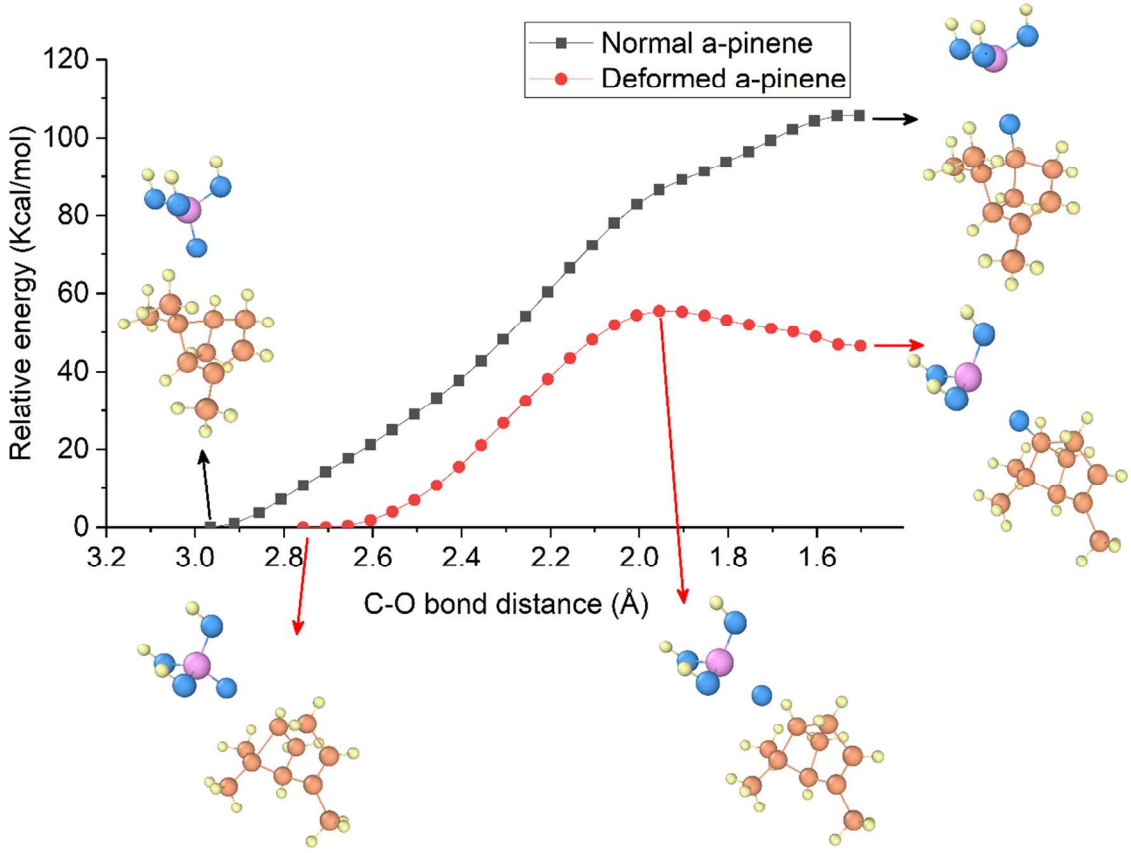

Figure S9. Energetics of the oxidative activation (O1 → C6) coordinate along which a slightly deformed α-pinene molecule (red line) reacts with a dangling oxygen of the silica surface (as shown in Figures 4b and 4c in the main text). The surface oxygen atom was modeled as an isolated $(HO)_3Si$-O species for simplification in the energy calculation. The activation barrier is lower compared to the same reaction of an undeformed α-pinene in its equilibrium structure (blue line).

To check the effect of deformation of a-pinene molecule on the polymerization of a-pinene, we performed a series of ReaxFF MD simulations using simple geometries.

Figure S9 represents the donation of O from $(HO)_3Si$-O to C6 of normal & strained a-pinene. The reaction of C6-O formation for normal pinene is uphill reaction with 105.9 kcal/mol, while the energy barrier of C6-O bond formation for deformed pinene is 55.58 kcal/mol. This is because the O donation creates relatively larger bond & angle strain with overcooridnated C atom for normal a-pinene. On the other hand, thanks to distorted / broken structure, bond of dangling Oxygen was more favorable for deformed a-pinene than a normal one.

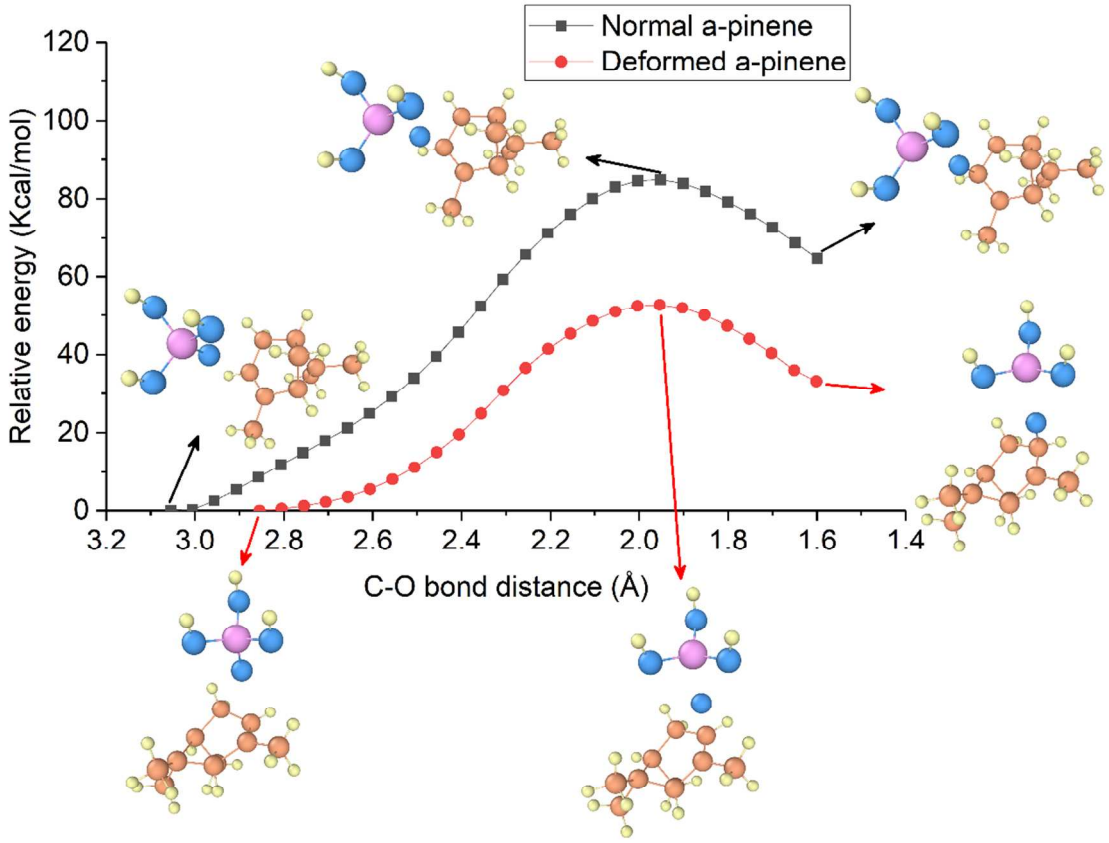

Figure S10. Comparison of the energetics for an oxidative activation step where a surface dangling oxygen (O1) is reacting with the one of the carbons in the double bond (C4) of α-pinene. The red and blue lines correspond to a slightly deformed and undeformed α-pinene molecule, respectively.

Similarly, as shown in Figure S10, the energy barrier for C4-O bond formation reaction of normal a-pinene was larger than deformed a-pinene. Energy barrier for oxygen donation to C4 site for normal pinene is 84.89 kcal/mol, while the energy barrier for deformed one is 51.93 kcal/mol. The deformed a-pinene molecule contains more atomistic angle/bond strain energy for the atoms around C4, which caused the lower energy barrier for C-O bond formation.

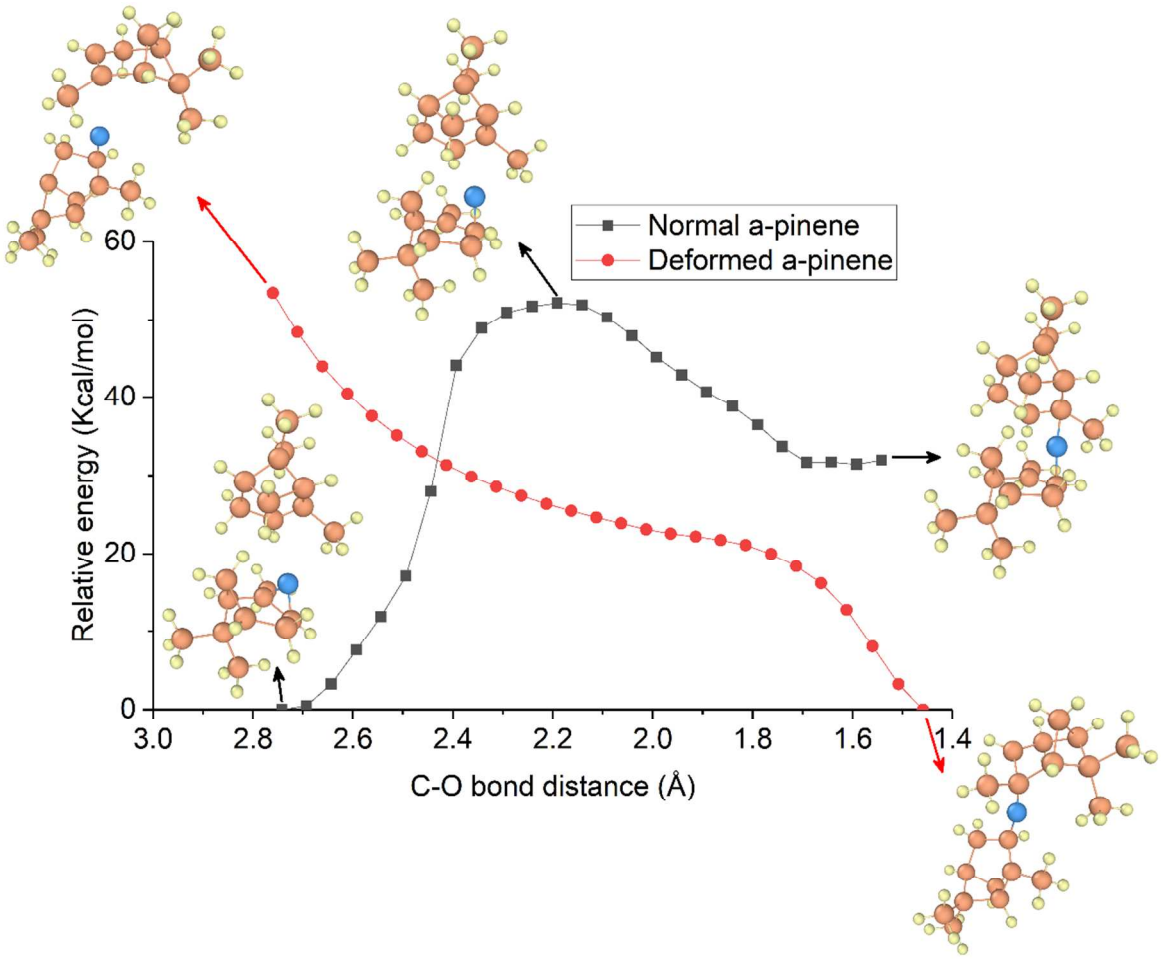

Figure S11. Energetics for the reaction between an oxygen radical at the C4 position of one α-pinene and the C3 carbon of another α-pinene. In the case of the deformed α-pinene intermediate (red curve), the initial state is so unstable and reactive that there is no activation barrier. In contrast, the fully relaxed intermediate (blue curve) shows an activation barrier for the same reaction.

Figure S11 depicts the oxygen transport and formation of C4-O-C3 connection between two a-pinene molecules. It is shown that the existence of a dangling oxygen on C4 for deformed a-pinene molecules are so unstable, that inducing a high initial relative energy at the beginning of reaction. As a result, the C4-O-C3 formation for deformed a-pinene is the downhill reaction. On the other hand, energy barrier of C4-O-C3 formation with normal a-pinene is calculated as 52.15 kcal/mol. This shows that the deformed a-pinenes are more likely to accept the C-O-C connection with other a-pinene molecules.

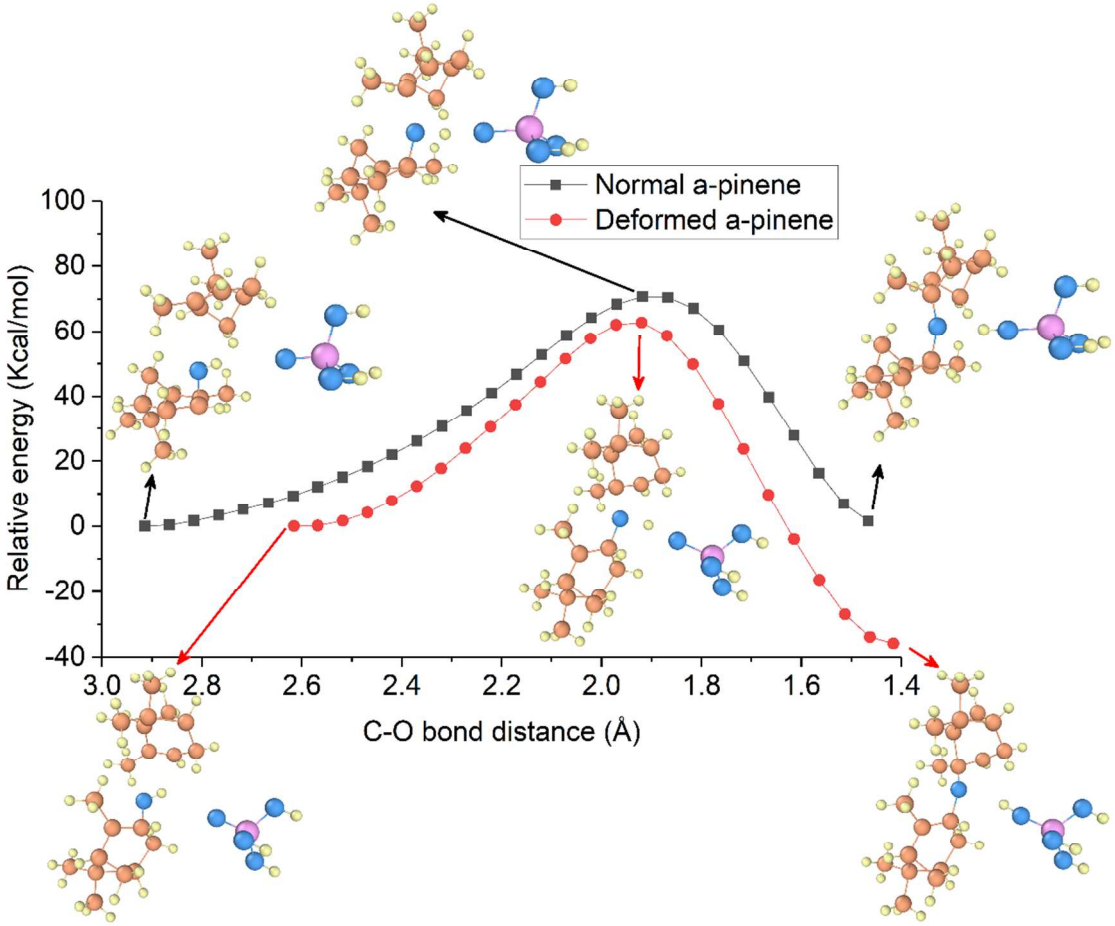

Figure S12. Energetics for the reaction between a hydroxyl group at the C4 position of one α-pinene and the C3 carbon of another α-pinene. In this scheme, the reaction proceeds first through donation of hydrogen from C3-O-H to a surface O-Si(OH)$_3$ species followed by formation of C3-O-C4 ether bond formation. The activation energy is slightly lower (by ~8 kcal/mol) for the deformed intermediate (red line), compared to the fully relaxed intermediate (blue line).

In figure S12, on top of the a-pinene molecule and hydroxylated a-pinene, O-Si(OH)$_3$ is introduced for the hydrogen donation. Here, we calculated the energy of H hopping from C3-O-H to O-Si(OH)$_3$, which will bring the formation of C3-O-C4 connection and Si(OH)$_4$. Our calculation shows that the deformed a-pinene case showed the 62.84 kcal/mol, while the normal a-pinene brings 70.76 kcal/mol. Like other examples, this calculation also proved that the energy barrier for the C-O-C formation reaction is lower for the deformed a-pinenes, than that of normal a-pinenes.

Distribution of oxygen atoms in the shear-induced association reaction products

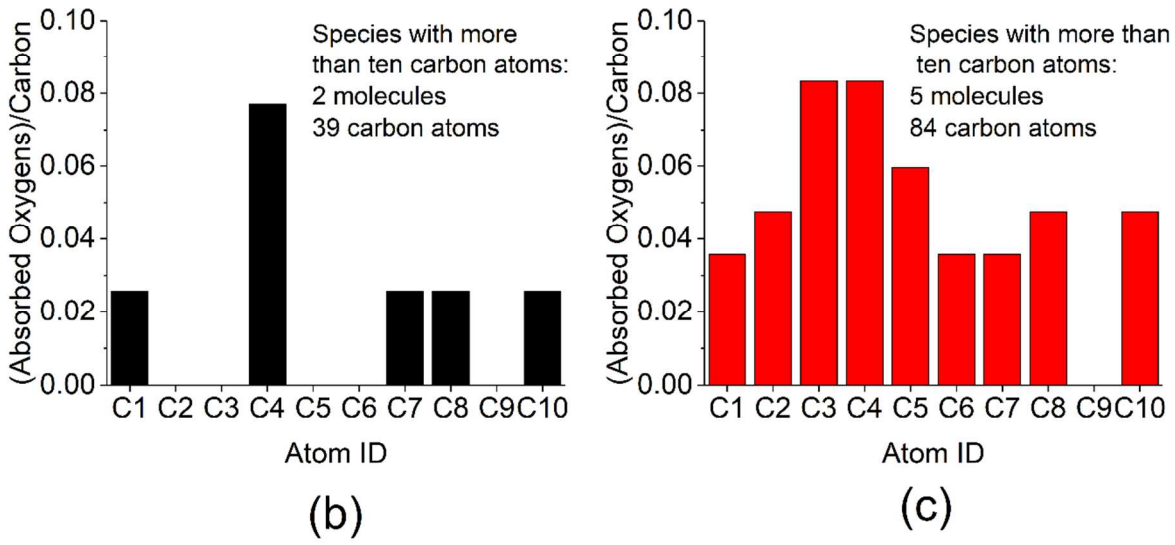

Figure S13. Regio-selectivity in oxidative activation of carbon atoms in reaction products containing more than ten carbon atoms in MD simulations at a contact pressure of 1 GPa for (a) hydroxylated and (b) non-hydroxylated silica surfaces.

References

(1) Smith, D. K. Opal, cristobalite, and tridymite: noncrystallinity versus crystallinity, nomenclature of the silica minerals and bibliography. *Powder diffraction* **1998,** *13* (1), 2-19.

(2) Stachurski, Z. H. On Structure and Properties of Amorphous Materials. *Materials* **2011,** *4* (9), 1564-1598, DOI: 10.3390/ma4091564.

(3) Yeon, J. *Development of a reaxff reactive force field for silicon/oxygen/hydrogen/fluoride interactions and applications to hydroxylation and friction*, The Pennsylvania State University: 2016.

(4) Mozzi, R.; Warren, B. The structure of vitreous silica. *Journal of Applied Crystallography* **1969,** *2* (4), 164-172.

(5) Zhuravlev, L. The surface chemistry of amorphous silica. Zhuravlev model. *Colloids and Surfaces A: Physicochemical and Engineering Aspects* **2000,** *173* (1), 1-38.

(6) Gosvami, N.; Bares, J.; Mangolini, F.; Konicek, A.; Yablon, D.; Carpick, R. Mechanisms of antiwear tribofilm growth revealed in situ by single-asperity sliding contacts. *Science* **2015,** *348* (6230), 102-106.

(7) Vahdat, V.; Ryan, K. E.; Keating, P. L.; Jiang, Y.; Adiga, S. P.; Schall, J. D.; Turner, K. T.; Harrison, J. A.; Carpick, R. W. Atomic-scale wear of amorphous hydrogenated carbon during intermittent contact: a combined study using experiment, simulation, and theory. *Acs Nano* **2014,** *8* (7), 7027-7040.

(8) Jacobs, T. D.; Carpick, R. W. Nanoscale wear as a stress-assisted chemical reaction. *Nature nanotechnology* **2013,** *8* (2), 108-112.

(9) Jacobs, T. D.; Gotsmann, B.; Lantz, M. A.; Carpick, R. W. On the application of transition state theory to atomic-scale wear. *Tribology letters* **2010,** *39* (3), 257-271.

(10) Bell, G. I. Models for the specific adhesion of cells to cells. *Science* **1978,** *200* (4342), 618-627.

(11) He, X.; Kim, S. H. Mechanochemistry of Physisorbed Molecules at Tribological Interfaces: Molecular Structure Dependence of Tribochemical Polymerization. *Langmuir* **2017,** *33* (11), 2717-2724.